ORIGINAL PAPER

Spatial seismic response of non-uniform wide river valley with multistage slopes in lower reaches of Yangtze River

Li Xiaoxiong[1,2] · Zhuang Haiyang[2,3] · Li Zhaoyan[1] · Lu Lintong[2] · Zhao Kai[2]

Abstract

The geological conditions of the wide river valley in the lower reaches of the Yangtze River are characterized by complex site conditions due to the presence of multistage slopes and non-uniform stratigraphy. Considering such conditions, a finite element analysis model for multistage slopes in wide river valleys was developed. The model is based on the ABAQUS software platform, and a viscoplastic memorial nested yield surface model of soft soil is used to simulate the nonlinear dynamic properties of soils. The spatial variability characteristics of the seismic response at different depths of stratigraphy and the ground surface under the influence of traveling wave and overlying water pressure are investigated. Results show that the seismic response at different locations on the ground surface of the river valley site varies significantly, and the change pattern is consistent with topographic relief. The seismic response produces abrupt changes at the top of the multistage slopes, topographic relief, and lenticular body. The response spectrum of the ground surface exhibits characteristics of multiple peaks and a strong response over a wide range of periods, and the peak acceleration at the bottom of the river valley on both sides exceeds that on the ground surface. A comparison between the calculated and simplified model results ignoring topographic relief and soil non-uniformity further reveals the spatial variability of the seismic responses of the non-uniform wide river valley site.

Introduction

Numerous seismic records and observed earthquake damage confirm that topographic effects exacerbate the extent of earthquake damage to buildings (Gaudiosi et al. 2021; Wang et al. 2021a; Primofiore et al. 2020; Wei and Yang 2019; Hough et al. 2010; Ashford and Sitar 1997). Local irregular topography can cause seismic wave scattering, leading to superposition between incident and scattered waves and causing further attenuation, amplification, and spatial variations in ground motions (Gao et al. 2022). A river valley, a common depressed local irregular terrain, not only amplifies ground motion intensity during vibrations but also causes spatial variation of ground motion within the local site (Li et al. 2022). The "Guidelines for Seismic Design of Highway Bridges" (JTG/TB02-01–2008) stipulates that the evaluation of seismic safety must consider the spatial variation of ground motion caused by the local site and traveling wave effects. Thus, the seismic responses of bridges and tunnels that cross-river valley sites have particularities and complexities. Therefore, an investigation of the spatial variation characteristics of the seismic response of local irregular sites of river valleys can further improve the scientificity and reliability of aseismic calculations for large foundation projects at such sites.

Ground motion amplification was first recorded at the shoulder of Pacoima Dam in the USA in 1971 (Trifunac and Hudson 1971). Subsequently, countries began to deploy numerous seismic arrays to study topographic effects further. In the 1992 Hualien earthquake, a significant topographic effect was observed by strong-motion seismographs in Emerald River Valley, Taiwan Province, China (Huang and

✉ Zhuang Haiyang
  zhuang7802@163.com

1. Key Laboratory of Earthquake Engineering and Engineering Vibration, Institute of Engineering Mechanics, China Earthquake Administration, Harbin 150080, China

2. Institute of Geotechnical Engineering, Nanjing Tech University, Nanjing 210009, China

3. School of Civil Engineering and Architecture, East China Jiaotong University, Nanchang 330013, China

Chiu 1995). With the accumulation and collation of earthquake damage data from previous earthquakes, the topographic effects of river valleys have attracted the attention of scholars. Accordingly, extensive research has been conducted using analytical analysis (Zhang et al. 2021, 2019; Gao et al. 2012), numerical methods (Liu et al. 2022, 2018; Evangelista et al. 2017), and strong ground motion observations (Malcioglu et al. 2022; Lashgari and Jafarian 2022; Xie et al. 2017). The analytical method simplifies the river valley model in problem analysis; however, it cannot comprehensively consider the influence of soil mechanical properties and river valley shape. The strong ground motion observation method requires actual seismic measurement data; however, current seismic records are limited, and seismic records may not exist for some specific sites. Therefore, the analytical and strong ground motion observation methods are relatively limited. With advancements in computer technology and numerical calculation theory, numerical methods have become an important means for investigating the topographic effects of local irregular sites, and have achieved a relatively rich research results (Baron, et al. 2022; Chen, et al. 2021; Jahromi and Karkhaneh 2019; Ning, et al. 2018; Wang, et al. 2015; Hayashi, et al. 2001). Presently, most of the model section shapes studied are focused on deep V-shaped and U-shaped river valleys (Lopez-Castaneda and Reinoso 2021), whereas only a few studies are related to the unique site of wide river valleys. The sites in the middle and lower reaches of the Yangtze River are all wide river valleys, and numerous large engineering structures have been and are to be built on such sites. Accordingly, the investigation of the spatial variability characteristics of the seismic response of local irregular wide river valley sites in the lower reaches of the Yangtze River using numerical methods has practical importance.

In existing research, when numerical methods are used for analyzing the topographic effect of river valley sites, the real site topographic features and non-uniform spatial distribution of soil layers are simplified; hence, they are not fully considered (Wang et al. 2021b; Sohrabi-Bidar et al. 2010). Elgamal et al. (Elgamal et al. 2005, 2009; Li et al. 2020) presented finite element analysis with refined 2D and 3D non-uniform and nonlinear models, not only for soils but also for soil-structure interactions. However, the multistage slopes of and soil distribution in river valleys have important topographic effects (Gao et al. 2012). The wide river valley in the middle and lower reaches of the Yangtze River has wide multistage terraces and floodplains, and the sedimentary layer has numerous lenses (Wang et al. 2005). The foregoing indicates the topographic complexity and stratigraphic specificity of wide river valleys in the middle and lower reaches of the Yangtze River. Therefore, to investigate the spatial variability characteristics of the seismic response of the wide river valley sites in the middle and lower reaches

of the Yangtze River, the non-uniformity of the soil layers and topographic characteristics of the sites must be fully considered.

In summary, a multistage slopes finite element analysis model was developed for wide river valleys, specifically for a site in the lower reaches of the Yangtze River where a cross-river electric power-integrated pipe gallery is located. The design of the model was based on the engineering background of the site. Moreover, the effects of traveling wave and overlying water pressure are fully considered in the model. The dynamic nonlinear properties of soil were also simulated by using a previously developed viscoplastic memorial nested yield surface model of soft soil. The spatial variation characteristics of the seismic response of the site in the wide river valley are systematically examined to explore the topographic effect on the seismic response characteristics of the site further. Moreover, the calculation results are compared with the simplified model ignoring the effects of topography and non-uniform soil stratum. The results of the research provide a reference for the seismic design of cross-river project in the lower Yangtze River.

Engineering geology overview

The wide river valley site studied herein is located near the frontal zone of the delta plain in the lower reaches of the Yangtze River, which has wide multistage terraces and floodplains. A considerable amount of sand is transported to the lower Yangtze River and deposited every year, forming a thick and loose Quaternary Holocene fluvial–lacustrine alluvium on the terrace that has a typical binary-layer sedimentary rhythm structure (Zhuang et al. 2018; Wang et al. 2005). The topography of the river valley considerably fluctuates along the north–south direction. The slope of the south bank is lower than that of the north bank, and the soil layer of the south bank is looser, as shown in Fig. 1. The engineering site is divided into four classifications based on the equivalent shear wave velocity of the soil layer at a depth of 20 m and the thickness of the site overburden. The foregoing is based on the relevant regulations of the Chinese Code for Seismic Design of Buildings (GB50011-2010, 2016). The geotechnical engineering investigation report indicates that the conditions of the site considered in this study are those of Class IV sites, as listed in Table 1.

Development of numerical model

Element meshing

A static–dynamic coupling finite element analysis model of the nonlinear seismic response of a non-uniform wide river
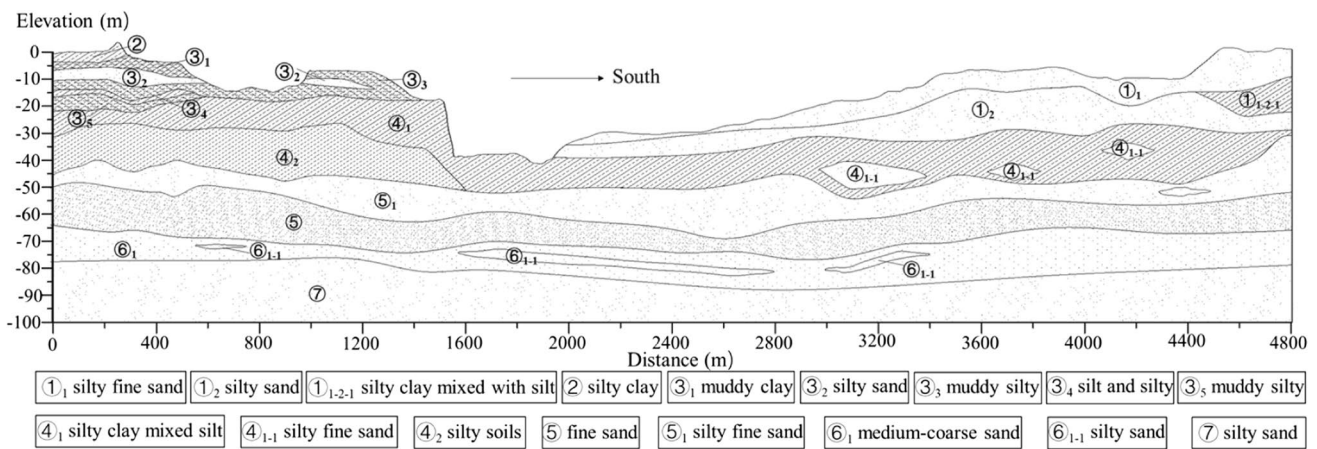
Fig. 1 Soil layer distribution in the wide river valley site

Table 1 Class IV site conditions

Site classification	Soil thickness, d (m)	V_{20} (m/s)	Classification criterion
IV	> 80	141	$d \geq 80$ and $V_{20} \leq 150$

valley is formulated based on the site shown in Fig. 1 that is fully consistent with the actual site (Fig. 2). The width and depth of the model are 4800 and 100 m, respectively. The size of the soil element mesh is determined using the following (Kuhlemeyer and Lysmer 1973; Zhuang et al. 2021):

$$h = \left(\frac{1}{10} - \frac{1}{8} \right) \frac{V_s}{f_{max}}, \tag{1}$$

where f_{max} is the cutoff frequency, and V_s is the least shear wave velocity in all soil layers. In this study, the high-frequency end (f_{max}) is set to 9 Hz, and the size of the soil element mesh is approximately 1 m. The model has numerous soil elements. To improve computational effectiveness, four-node bilinear plane strain quadrilateral reduced integration elements (CPE4R) are used.

The accurate geometry model was obtained from a CAD drawing of the site provided in the geotechnical investigation report, as shown in Fig. 1. In the present study, a CAD drawing was imported into Abaqus/CAE to generate the numerical model, as presented in Fig. 2. Hence, the soil distribution is uneven along the north–south direction. Moreover, soil interfaces, lenticular bodies, and large topographic undulations exist. The use of a uniform size of meshes at these locations is problematic. However, an excessive variation in the shape of the soil element mesh leads to considerable errors, reducing the accuracy of the calculation results. The triangular and trapezoidal meshes were used for the transition. Following the automatic mesh generation by the software, several element distortions were corrected by manually adjusting the node coordinates of a few elements. The resulting model mesh is displayed in Fig. 3.

In existing analysis methods, the static analysis step and the dynamic analysis step are analyzed separately, and then, the calculation results of two steps are added together. Such methods are unable to consider the influence of the initial geostatic stress on the dynamic properties of soil. Because the underground station is buried in soil, the initial geostatic stress conditions of the surrounding soil will have a significant impact on the dynamic characteristics. To address the problem, a static-dynamic coupling finite element analysis model was developed by Zhuang et al. in 2011. In the model, before performing the dynamic analysis step, the static stress state is calculated and the dynamic shear modulus of the soils is updated based on the static confining stress. In addition, the static and dynamic analysis steps are coupled together (Zhuang et al. 2011 and 2019). In the present study, the finite element analysis method was used to consider
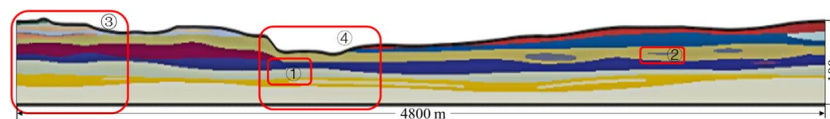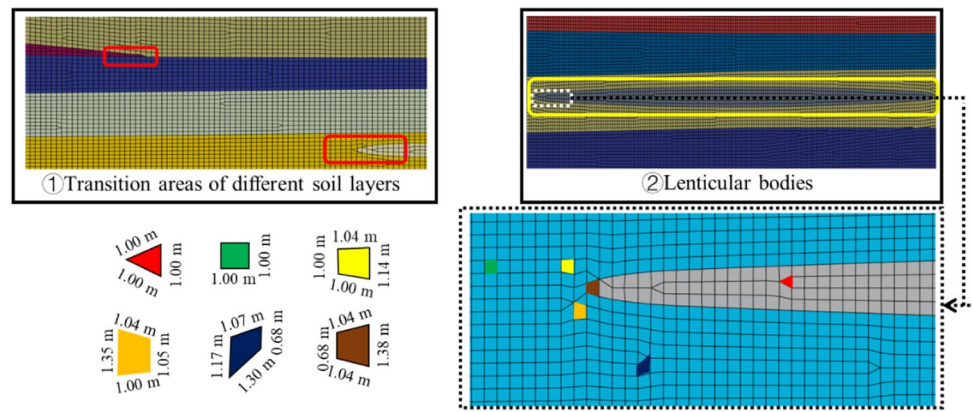

Fig. 2 Numerical model: (1) transition areas of different soil layers; (2) lenticular bodies; (3) local uneven site; (4) U-shaped field at valley bottom

Fig. 3 Finite element meshing of soil

the influence of the initial geostatic stress of soil, so as to explore the differences between the non-uniform wide river valley site and simplified model. Based on the distribution of soil layers in a section of the wide river valley site, the simplified model extends to a certain width on both sides in the horizontal direction. In the simplified model, each soil layer has the same thickness, and the slope of the ground surface is 0°. The influence of the model boundary can be eliminated if the ratio of the model width (L) to soil depth (h) exceeds 20, i.e., $L/h > 20$ (Wang et al. 2021c); accordingly, the width of the built model is 2000 m. The model shown in Fig. 4 is simplified based on the right cross-section of area (3) in Fig. 2. The schematic is only used to illustrate the method for building the simplified model considering several selected sections. Owing to the large domain of the numerical model, all the calculations were completed at the High Performance Computing Centre of Nanjing Tech University, which has 2784 CPUs that can be used for simultaneous calculations. The peak speed was 128.84 GFLOPS. In the study, 28 CPUs were allotted to calculate one model. As a result, it took approximately 4 days to complete one computing case.

Dynamic constitutive model of foundation soil

Under the cyclic loading, the shear modulus should degenerate with the number of cyclic loading and the dynamic deformation of soil should show the unidirectional accumulation property, which could not be simulated by the Mohr–Coulomb model or (modified) Cam-clay model. Due to the above problem, the viscoplastic memorial nested yield surface model of soft soil, established by Zhuang (Zhuang and Chen 2006 and Zhuang et al. 2020), was used in this study as a nonlinear dynamic constitutive model. According to the deformation characteristics of soft soil under the dynamic loading, the mixed hardening modulus field theory combining the isotropic hardening and dynamic hardening is adopted. That is, the inverted loading surface f_r, the failure surfaces F, and the initial loading surface f which were concenter with the inverted loading surface f_r were memorized, and then, the loading yield surface f is internally tangent with the inverted loading surface f_r, as presented in Fig. 5. The spatial position of the initial yield surface is determined by a. When $a = 0$, the soil is considered the initial isotropic material; conversely, when $a \neq 0$, the initial anisotropy of the soil is considered. In order to consider the viscosity effect of the soil, the Rayleigh damping is introduced into the expression of the stress–strain relationship of the constitutive model. The first step in the ABAQUS algorithm is to input the internal friction angles, densities, shear wave velocities, and Poisson's ratios of the different soils.

The feasibility of the dynamic constitutive model is verified by dynamic triaxial tests. Moreover, it was successfully applied to the calculation and analysis of the nonlinear seismic responses of actual project sites (Yang et al. 2021). The
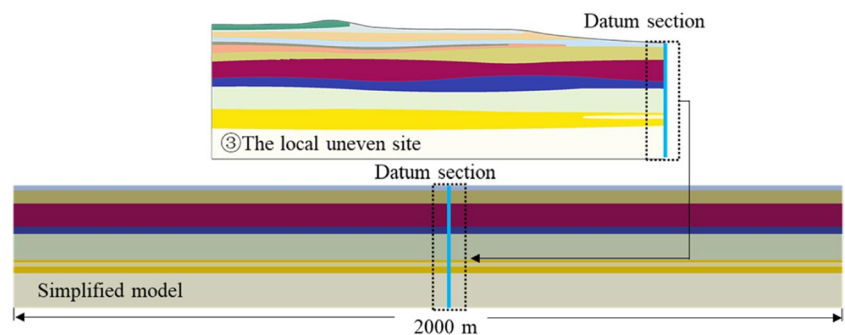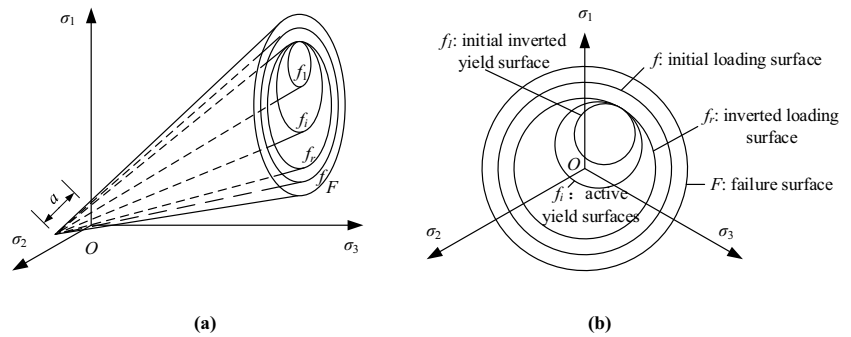
Fig. 4 Simplified model

Fig. 5 Yield surfaces in the principal stress space and the deviatoric plane. **a** The yield surfaces in stress space. **b** The yield surfaces in deviatoric plane

(a)

(b)

drainage model of foundation soil is not considered in the calculation; accordingly, the dynamic Poisson ratio of the soil layers is set to 0.49. The parameters presented in Table 2 were obtained from the geotechnical investigation report for the Sutong GIL pipe gallery engineering project. G_0 represents the maximum initial shear modulus of the soil, which is determined by $G_0 = \rho \cdot v_s^2$, where ρ and v_s are the density and shear wave velocity of the soil layer, respectively.

Treatment of boundary

The treatment of model boundaries is critical for accurate seismic response analysis of a site. However, due to the complex geological conditions of the Yangtze River, there are difficulties in weakening the reflective waves generated by non-homogeneous soil layers in multiple directions using the analytical boundary treatment method. To overcome such issue, the lateral boundaries of the finite element model in the present study were set to be wider than the main wide river valley, so as to weaken the reflective waves from the lateral boundaries by the additional lateral soils. The treatment of the model boundary includes static and dynamic analyses. (1) A fixed constraint is adopted for the bottom boundary of the foundation. In the static analysis step, the lateral boundary is horizontally constrained and vertically free. After the static analysis, ground stress balance is implemented based on the static calculation results. (2) In the dynamic analysis, the lateral boundary is horizontally free and vertically constrained. The horizontal support reaction force of the lateral boundary obtained by static analysis is applied to the corresponding nodes in the form of concentrated force. The horizontal constraint of the bottom boundary of the foundation was replaced by the input horizontal ground

Table 2 Fundamental physical and mechanical parameters of soil layer in wide river valley

Soil	Maximum initial shear modulus G_0 (MPa)	Weight (kN/m³)	ϕ (°)	Young's modulus (MPa)	Poisson's ratio, v	Shear wave velocity, v_s (m/s)
①₁ silty fine sand	33	19.6	34.2	4.5	0.37	130
①₂ silty sand	63	19.3	28.0	4.5	0.34	180
①₁₋₂₋₁ silty clay mixed with silt	47	18.3	33.9	7.8	0.34	160
② silty clay	109	18.9	24.7	2.3	0.37	240
③₁ muddy clay	18	18	21.3	1.5	0.39	100
③₂ silty sand	49	19.3	31.2	3.9	0.34	160
③₃ muddy silty clay	46	18.1	19.9	1.5	0.39	160
③₄ silt and silty clay	114	18.3	25.3	6.5	0.34	250
③₅ muddy silty	46	18.0	23.6	2.5	0.39	160
④₁ silty clay mixed silt	59	18.1	24.5	5.2	0.34	180
④₁₋₁ silty fine sand	172	19.1	35.2	9.2	0.29	300
④₂ silty soils	123	18.2	28.6	10.5	0.32	260
⑤₁ silty fine sand	201	19.6	34.0	22.9	0.29	320
⑤ fine sand	216	19.8	33.6	40.9	0.26	330
⑥₁ medium-coarse sand	220	20.2	35.2	48.0	0.27	330
⑥₁₋₁ silty sand	250	19.3	38.2	37.5	0.25	360
⑦ silty sand	304	20	31.6	26.0	0.34	390

motion. The boundary transformation process is illustrated in Fig. 6.

Selected ground motion and calculated working conditions

The selection of a suitable ground motion is important for investigating the dynamic response of the non-uniform wide river valley (Bao et al. 2021; Zhu et al. 2022). During the Kobe earthquake (magnitude 6.9) in Japan in 1995, Kobe motion was recorded by the KJMA station. The thickness of the sediment layer at the station site and the non-uniform site studied in this paper are both about 100 m. Moreover, the earthquake caused numerous geological disasters and destroyed urban underground structures. This event prompted the rapid promotion of research on earthquake-resistant engineering structures. Scholars have used the Kobe motion as input ground motion to study the mechanism of geological disaster occurrence and achieved considerable research results (Sahoo and Shukla 2021; Nguyen et al. 2020; Yang, et al. 2020; Zhuang et al. 2020; Rietbrock 2001). Gao et al. (2018) analyzed the effect of pulse ground motion on the site shear characteristics, and found that the three-dimensional pulse ground motion could be appropriately simplified as the horizontal direction. Moreover, Fukushima et al. (2000) generated a map of horizontal peak-ground acceleration in the Kobe and Osaka area for the Kobe earthquake based on the corrected attenuation relation for the site condition effect. The simulated results exhibited

good agreement with the area of severe damage categorized as intensity VII on the JMA scale. Hence, in this study, the N-S component of the Kobe motion is selected as the bedrock input ground motion in which the peak moment occurs during the first 30 s. The ground motion acceleration time history curves and response spectra are shown in Fig. 7. The input ground motion intensity is adjusted to 0.15 g by adjusting the original peak acceleration; it is inputted horizontally to the bottom of the model foundation.

The width of the wide river valley site reaches 4800 m, and the ground motion propagation at the bottom of the foundation at different locations exhibits time asynchrony. Therefore, the traveling wave effect of the ground motion input must be considered. Consistent and non-consistent seismic wave inputs at the bottom of the model foundation are considered in this study. In the traveling wave analysis, the wave speed used is 1000 m/s. The nodes within 50 m of the foundation bottom form a set, and the traveling wave effect of seismic waves is simulated by inputting ground motions asynchronously among different node sets. The seismic response characteristics of wide river valley sites with and without overlying water pressure are compared, and the difference between the simplified and refined models is analyzed. Huang et al. (Huang and Zhu 2017; Zhu and Huang 2017) equated the hydrodynamic pressure to joint mass exerted on the water-panel interface. As such, the overlying water pressure is simplified as hydrostatic pressure in the simulation, and the interaction of fluid–solid coupling is not considered. The calculation conditions are listed in Table 3.

Fig. 6 Transformation settings of boundary conditions: **a** boundary condition in static analysis step; **b** boundary condition changed; and **c** boundary condition in dynamic analysis step
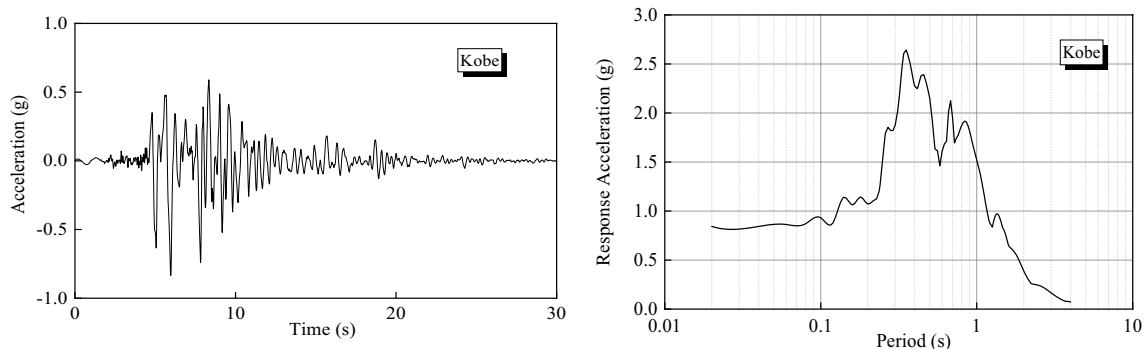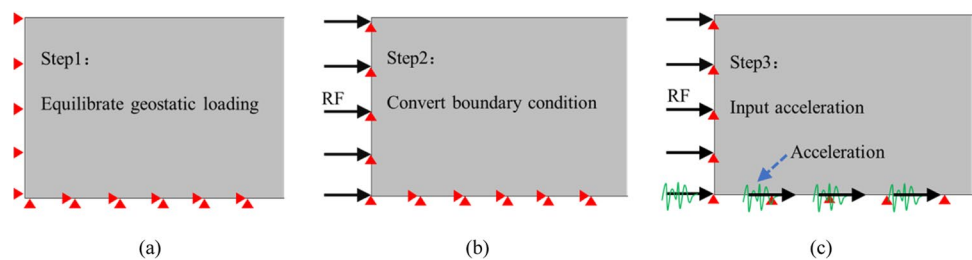

Fig. 7 Time history and acceleration response spectra of ground motion

Table 3 Calculated working conditions

Working condition	uT-uO-I	uT-O-I	T-O-I	T-uO-I	uT-uO-uI
Traveling wave effect	✗	✗	✓	✓	✗
Overlying water pressure	✗	✓	✓	✗	✗
Inhomogeneous soil	✓	✓	✓	✓	✗

Spatial variability of seismic response

Owing to the complexity of the topography and non-uniformity of soil layers, the propagation of ground motions in a wide river valley site considerably differs from that in a conventional site. In small areas, ground motion with engineering significance significantly varies. The topographic effect modifies the peak ground acceleration (PGA) and response spectrum at each point in the site (Anquez et al. 2022). Accordingly, PGA, peak ground velocity (PGV), and response spectral characteristics are selected in this study to analyze the spatial variability characteristics of the seismic response of this non-uniform wide river valley site systematically.

The wide river valley has multistage slopes on both sides. Along the north–south direction, the slope and inclination direction constantly change, and the ground surface of the site is continuously undulating. According to existing seismic data, a sudden change in ground motion occurs in positions where the topography fluctuates significantly (Gao et al. 2022). Additionally, when the ratio of the distance from the boundary to the depth of the site soil was greater than 5, the effect of the model boundary could be ignored (Wang et al. 2021a). The focus of the present study was on the seismic response of the 500–4300-m section of the site. Therefore, 16 observation points located at the bottom and top of the slope were selected to investigate the spatial variation characteristics of seismic responses, as shown in Fig. 8.

PGA

One of the main indicators for evaluating the seismic response of an engineering site is the PGA. It is also an important input ground motion intensity indicator for the seismic calculations of projects, such as cross-river bridges. Therefore, Fig. 9 shows the PGAs of various observation points on the ground surface of the wide river valley site under different working conditions. The figure indicates that under the same ground motion excitation, the acceleration responses at different locations on the ground surface significantly vary. Furthermore, the variation pattern of the peak acceleration on the ground surface is similar to that of topographic relief. The PGAs under all four working conditions increase steeply at the location of abrupt topographic change, producing the focusing effect of ground motion. This phenomenon is particularly evident at observation point 5 located at the shoulder of the slope; the slope at this position is significantly greater than those at other locations. The PGA pattern variation is virtually the same in areas with flat topographies. The foregoing rules are consistent with the analysis results of existing the seismic response patterns of river valley sites (Wang et al. 2021c; Costanzo and Caserta 2019). Moreover, a certain magnitude increase is observed in the peak acceleration at a location on the ground surface corresponding to that of the lenticular body. Therefore, the topographic relief and non-uniformity of the soil layer lead to spatial variations in the peak accelerations in the wide river valley site.

By comparing the calculation results obtained under different working conditions in Fig. 9, the peak accelerations with the water pressure effect (uT-O-I and T-O-I) are observed to be greater than those under other working conditions. The peak acceleration difference under each working condition is largest at the south bank shoulder, indicating that the seismic response of the surface is more intense when water pressure is considered. This increased intensity is more evident at a location with large topographic relief. The input ground motion varies more drastically with topography and exhibits more distinct focusing effects. This phenomenon is consistent with the shaking table experimental results obtained by Han et al. (2020). The main reason for this phenomenon is that the seismic waves propagating in the soil layer generate reflected waves when they encounter surface fluctuations and variations in the soil layer. This leads to the mutual superposition of seismic waves and reflected waves. When the traveling wave effect is considered, the
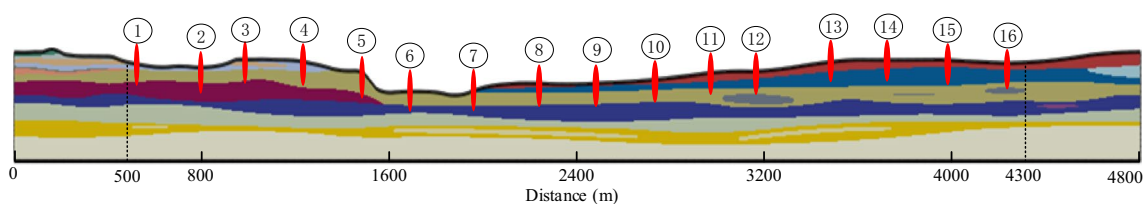

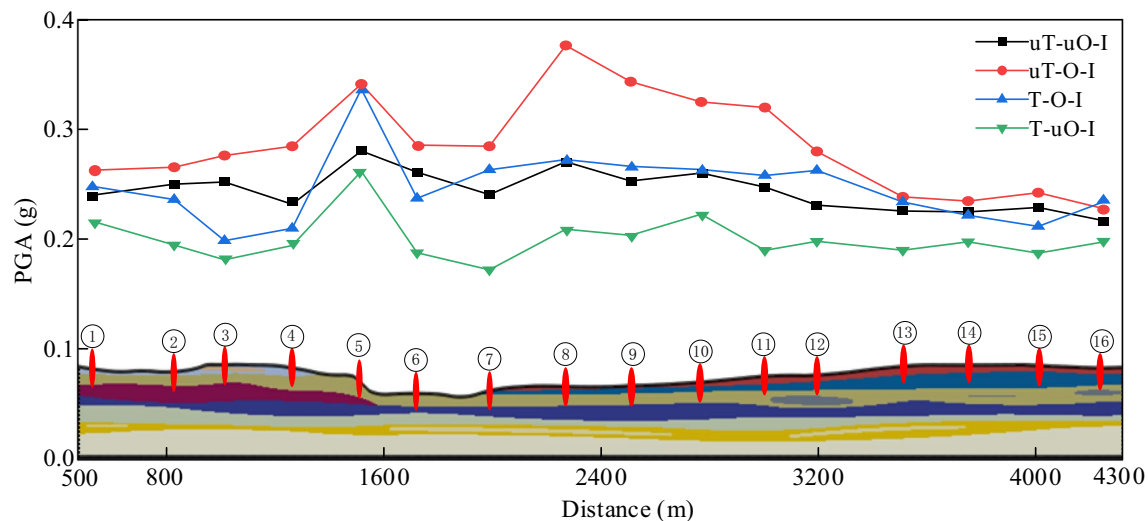**Fig. 8** Location of observation points in non-uniform wide river valley site

Fig. 9 Spatial differences in PGA

phase difference between seismic and reflected waves more closely approaches an odd number, causing the seismic waves to be more susceptible to mutual attenuation as they propagate through the soil layers.

To investigate the influence of the traveling wave and overlying water pressure on the site acceleration response further, Fig. 10 shows the acceleration cloud map of the 500–4300-m section of the wide river valley site when the acceleration at point 5 reaches its peak. As shown in Fig. 10, the acceleration cloud map of the wide river valley site indicates the occurrence of a stratification phenomenon due to the consistent ground motion input. The stratification pattern of the cloud map is similar to the soil layer distribution, and the acceleration cloud map pattern (neglecting the overlying water pressure) is similar to that of the soil layer with water pressure. The acceleration cloud map ceases to exhibit a stratification pattern along the north–south direction when the traveling wave effect is considered with the input ground motion; however, this absence in pattern is related to surface fluctuation. The peak value observed at the bottom of the river valley is the highest acceleration, and the peak acceleration of the north–south direction soil layer under the same burial depth constantly changes. Therefore, the ground motion input for non-uniform wide river valley sites (considering the traveling wave effect) has a considerable impact on the longitudinal earthquake resistance of shield tunnels and multistage pier bridges. However, the ground motion input when the traveling wave effect is neglected aggravates the extent of earthquake damage at different depths of the pier foundation.

The foregoing study results indicate that the acceleration responses at different locations on the site surface significantly vary, and the peak acceleration difference is greatest

near the bottom of the river valley. Therefore, to investigate the influence of non-uniform sites on seismic response further, the U-shaped local site area (4) shown in Fig. 2 is selected for the study (Fig. 11).

As shown in Fig. 11, the PGA change trend in the local U-shaped site is consistent with topographic relief: first increasing, then decreasing, followed by flattening, and finally increasing again. The PGA reaches its maximum at the shoulder of the north bank and then gradually decreases from the shoulder to the bottom of the slope. The PGA amplitude and change rate at the shoulder of the north bank exceed those at the shoulder of the south bank. This is mainly because the elevation and slope of the north bank are higher than those of the south bank (Taboada-Urtuzuastegui et al. 2002). From the top to the shoulder of the slope, the PGA exhibits a certain amplification trend. Therefore, when site selection is conducted for projects, such as dams, considering the impact of amplification in addition to the ground motion at the shoulder of the slope is necessary. The variations in PGA are relatively large under different working conditions; among these, PGA variations are the smallest and largest under the T-uO-I and uT-O-I working conditions, respectively. The PGA and its spatial variability under the two working conditions considering the overlying water pressure are larger than those of the two other working conditions. The main reason for the foregoing is related to the coupling of the overlying water pressure and topography. In this study, the river water is loaded on the surface in the form of water pressure. The dynamic coupling of river water-riverbed and the oscillation effect of water under the action of ground motion are ignored. However, during an actual earthquake, the foregoing influences the seismic response characteristics of the site. Therefore, the conduct of a study

Fig. 10 Site acceleration cloud map. (**a**) uT-uO-I; (**b**) uT-O-I; (c) T-O-I; (d) T-uO-I
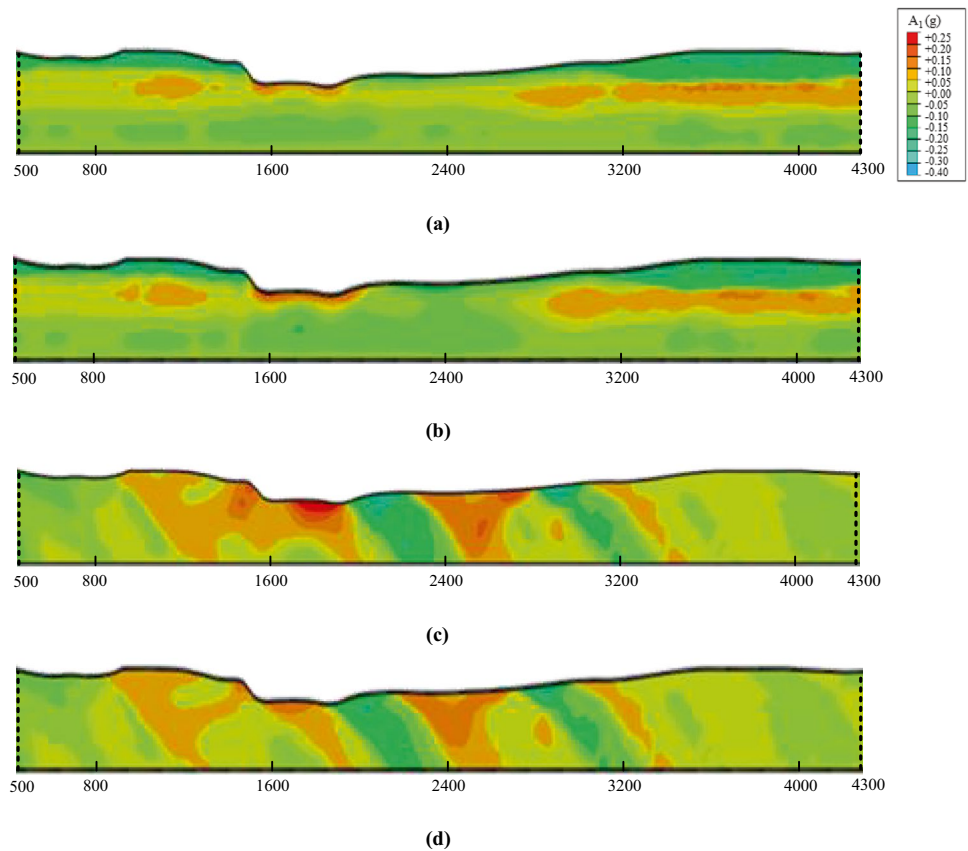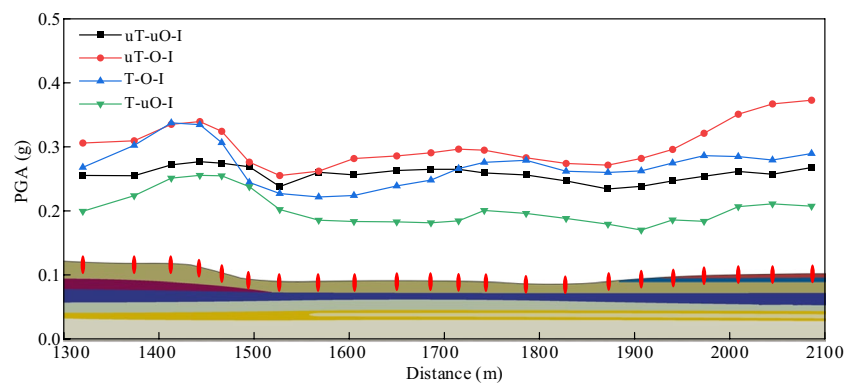

(a)

(b)

(c)

(d)

Fig. 11 PGA spatial differences at U-shaped field (4) in the valley bottom

on the seismic response of a wide river valley considering the effects of river water-riverbed coupling and river water oscillation is advantageous.

PGV

Another important indicator of seismic response is the PGV. It can be used to estimate the possibility of earthquake-induced landslides, assess site liquefaction potential, and rapidly assess post-earthquake disasters. Accordingly, the PGV distributions on the ground surface of the wide river valley and at the U-shaped local site (4) in Fig. 2 are plotted in this study, as shown in Figs. 12 and 13, respectively.

As shown in Fig. 12, the overall variations in PGV are small, and the change trend is consistent with the ground surface fluctuation. The PGV amplitude of the wide river valley site is mainly distributed in the range 30–40 cm/s, which is considerably less than the Kobe ground motion peak velocity of 162 cm/s. Therefore, the soil layer can be regarded as natural vibration damper and isolation layer. The PGV exhibits a distinct increasing trend at the shoulder on both sides of the slope. The ground surface is relatively wide at this location. The possibility of slippage at the shoulder of the slope during seismic safety evaluation must be considered. The PGV is maximum and minimum under the uT-O-I and T-uO-I working conditions, respectively. The possible
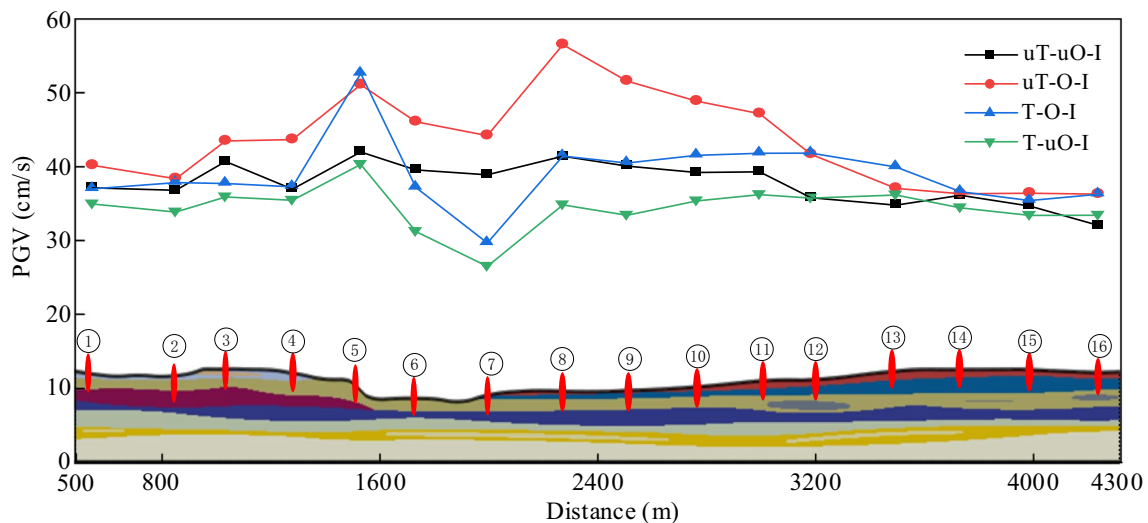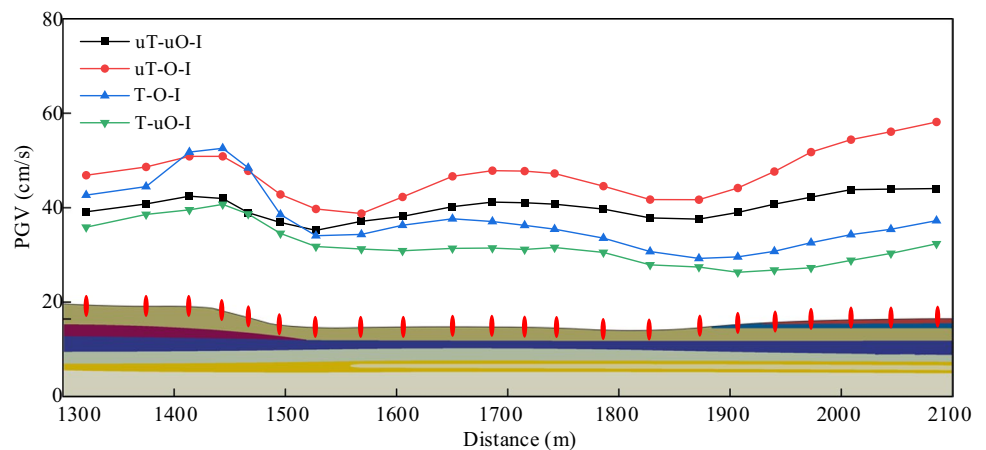
Fig. 12 Spatial differences in PGV

Fig. 13 Spatial differences in PGV at the U-shaped local site (4) in valley bottom

reasons for the above rule are related to the ground motion input, topographic relief, and mutual interference between the incident and scattered waves.

No abrupt PGV change is observed at the U-shaped local site shown in Fig. 13. The change in PGV on the ground surface of the site is gradual and relatively continuous among different locations. The PGV change rate at the top of the north bank slope under different working conditions varies. It leads to a continuous change in its size order; however, the PGV change trend near the top of the south bank slope is relatively consistent. The foregoing further phenomenon illustrates that the greater the topographic relief, the more complex the coupling effect between the different working conditions and topography. The PGV is smallest at the foot of the slope (both sides); it first increases and then decreases between the two sides at this location. This trend is the same as the PGA change pattern in the U-shaped local site.

As shown in Figs. 9, 10, 11, 12, and 13, a significant spatial difference in seismic response is observed on the ground surface of the non-uniform wide river valley site. The variation trend in the seismic response agrees with ground surface relief. However, abrupt changes in locations are mainly concentrated at the top of the multistage slope and at prominent positions on the ground surface. The least seismic response occurs at the foot of the valley bottom. The maximum and minimum seismic responses with respect to the PGA and PGV indices occur under the uT-O-I and T-uO-I working conditions, respectively. This phenomenon further illustrates the complexity of the seismic response of the wide river valley site. To a certain extent, the surface seismic response under different working conditions shows drastic changes near the area with relatively large ground surface relief. Therefore, consistent ground motion input cannot be simply adopted for the seismic design of major

engineering foundations crossing wide river valley sites; multi-point ground motion input with topographic effects must be considered.

Ground surface spectral response

The spectral characteristics of the soil layer are an important basis for determining whether major engineering structures across the river resonate under earthquake action. Accordingly, a total of 8 locations (points 5, 6, 7, 9, 11, 12, 15, and 16) with relatively large spatial variations in seismic response are selected. Furthermore, the spatial distribution of spectral characteristics on the ground surface of the non-uniform wide river valley site is investigated.

As shown in Fig. 14, the response spectrum at various observation points on the ground surface of the site exhibits a "multi-peak" phenomenon that differs from that of the homogeneous stratum, suggesting that the response spectrum of the ground surface is influenced by multiple strata. The range of periods corresponding to the occurrence of relatively large acceleration values at positions 11, 12, 15, and 16 is wide, indicating a high frequency of peak occurrence at these locations. However, the peaks of the spectral acceleration at locations 5, 6, 7, and 9 are larger than those

at other ground surface locations. By considering Fig. 8, the soil layer near the valley bottom is found to have relatively high peak spectral accelerations than those in other locations; however, the period range corresponding to the occurrence of relatively large acceleration values is narrower. The characteristic periods of the non-uniform wide river valley site are all approximately 1.0 s, and the acceleration response spectrum of the ground surface under different working conditions is less than 0.5 s. The variations among the acceleration response spectra of the ground surface under different working conditions increased continuously after 0.5 s, particularly when the period approached 1 s. In addition, most of the characteristic periods of the river-crossing bridges in the middle and lower reaches of the Yangtze River are approximately 1.0 s (Li et al. 2015), and the variability of the peak spectral acceleration corresponding to different ground surface locations when the period is 1 s is considerable. The seismic response of such sites may have an extremely adverse effect on the seismic responses of bridges. Accordingly, seismic analysis of such bridges must be considered.

The peak acceleration of the response spectrum is generally large when considering the overlying water pressure; this observation is consistent with the PGA response results.
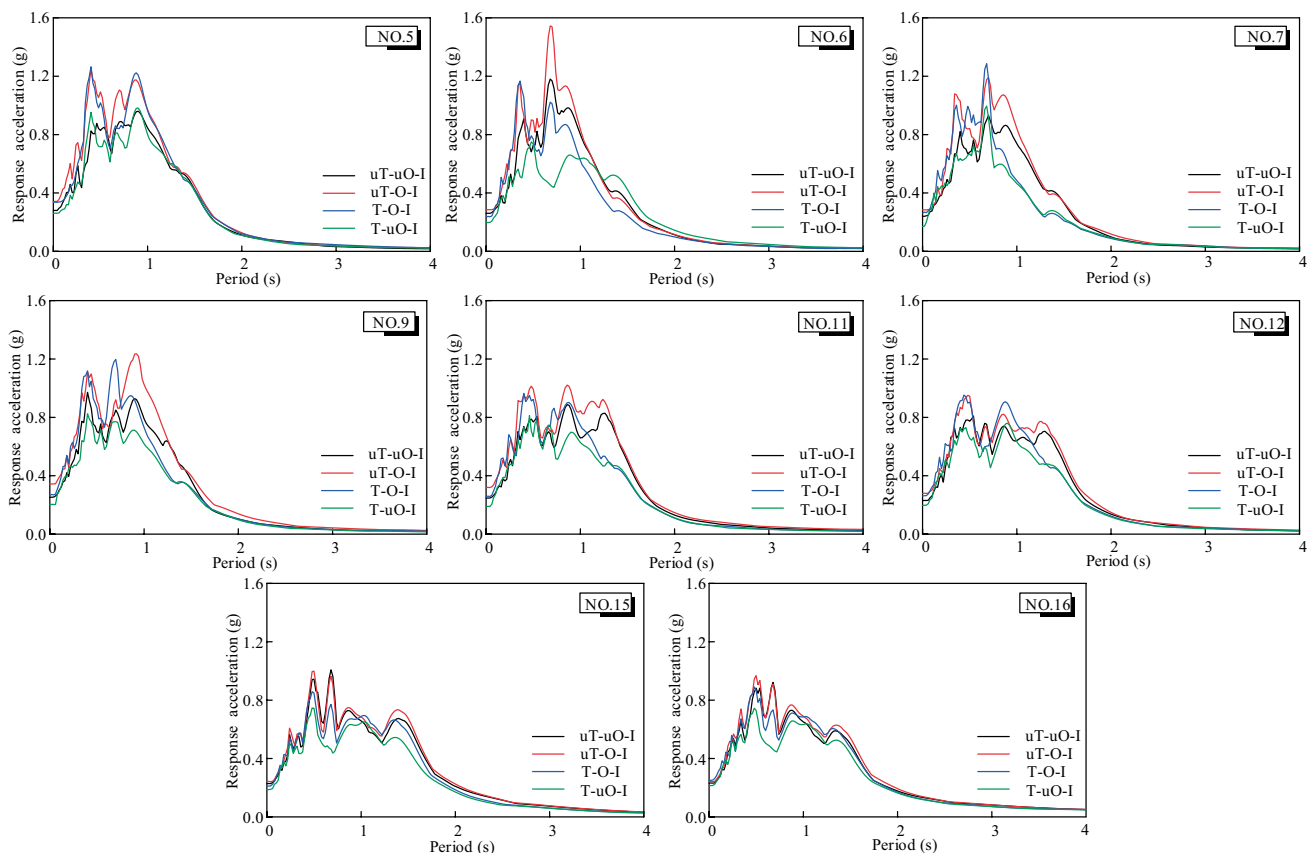

Fig. 14 Spectral characteristics of site ground surface

The peak acceleration of the response spectrum under consistent excitation exceeds that under traveling wave excitation, except for observation point 7. Notably, the peak acceleration at observation point 5 exceeds that at point 6, as shown in Fig. 9. However, based on the response spectrum, the peak acceleration at point 6 exceeds that at point 5. Therefore, important engineering projects crossing wide river valley sites are likely to sustain considerable structural damage at the valley bottom than at the top of the slope when the structures resonate with the soil during earthquakes.

Acceleration response along depth

This study comprehensively considered the non-uniformity of the topography and soil layer. To explore the variation rule of the seismic response along the depth of the soil layer, 11 sections are selected, as shown in Fig. 15. The site peak acceleration along the soil depth direction for the 11 sections from the bottom of the model foundation to the ground surface is shown in Fig. 16.

As shown in Fig. 16, the peak acceleration non-monotonically increases from the bottom of the model foundation to the ground surface; overall, it first decreases and then increases. The four working conditions selected in this study satisfy this rule. The acceleration decays when the ground motion propagates from the bottom of the model foundation to the silty sand bottom layer. Furthermore, the peak acceleration exhibits different rates of increase in various soil layers as the ground motion continues to propagate upward. However, the increase in peak acceleration amplitude at different depths at Sections 4 and 5 in calculation results of different models is approximately linear, and the sections are all located at the valley bottom. At other sections, the increasing trend of the peak acceleration exhibits a distinct nonlinearity. At a burial depth of 20 m, the peak acceleration exhibits a sharp increase. The properties and thicknesses of soil layers in Sections 10 and 11 are fundamentally the same. Section 11 has a lenticular layer 60 m from the bottom of the model foundation. The nonlinear characteristics of peak acceleration are observed to be more significant at this location. Therefore, the seismic design of multi-pier-specific bridges or shield tunnel structures in wide river valley

sites must focus on the variability of the structural seismic response at locations 20 m below the ground surface as well as at the valley bottom and location of lenses.

The effect of overlying water pressure on the peak acceleration at different depths of the soil layer is negligible at Sections 1–3 and 9–11. However, a difference in the degree of influence under various excitation modes of ground motion indicates that the peak accelerations under traveling wave excitation are generally smaller than those under consistent excitation. This rule agrees with that of the site's acceleration cloud map, as shown in Fig. 10. The peak acceleration along the soil depth direction under the influence of overlying water pressure significantly differs from those at Sections 4–8. Overall, the peak acceleration along the depth direction of the soil layer is minimum under the T-uO-I working condition, and the changes in peak acceleration amplitude are most evident under the uT-O-I working condition.

Variations in calculation results of different models

Differences in ground surface response spectrum

To investigate the spatial differences between the refined model considering the non-uniform soil stratum and the model with simplified horizontal soil strata, the ground surface response spectra of observation sites 2, 6, 12, and 16 are plotted in Fig. 17.

As shown in Fig. 17, the response spectra of the refined and simplified models exhibit various patterns at different observation points. The peak acceleration of the simplified model response spectrum at point 2 occurring between 0.7 and 1.5 s slightly exceeds that of the refined model. The characteristic period of this point is 0.5 s; however, that of the simplified model is 1.3 s. The pattern of the response spectrum at observation point 6 is opposite that of point 2. The characteristic period calculated by the refined model is smaller than that estimated by the simplified model; however, the peak spectrum acceleration of the refined model exceeds that of the simplified model. The characteristic
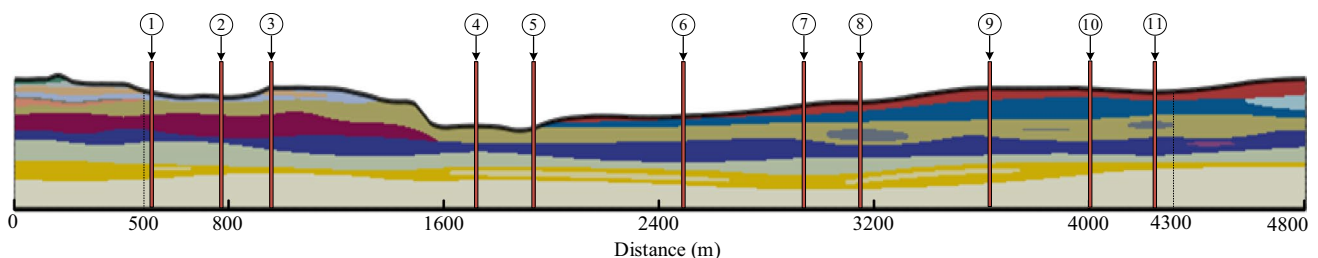

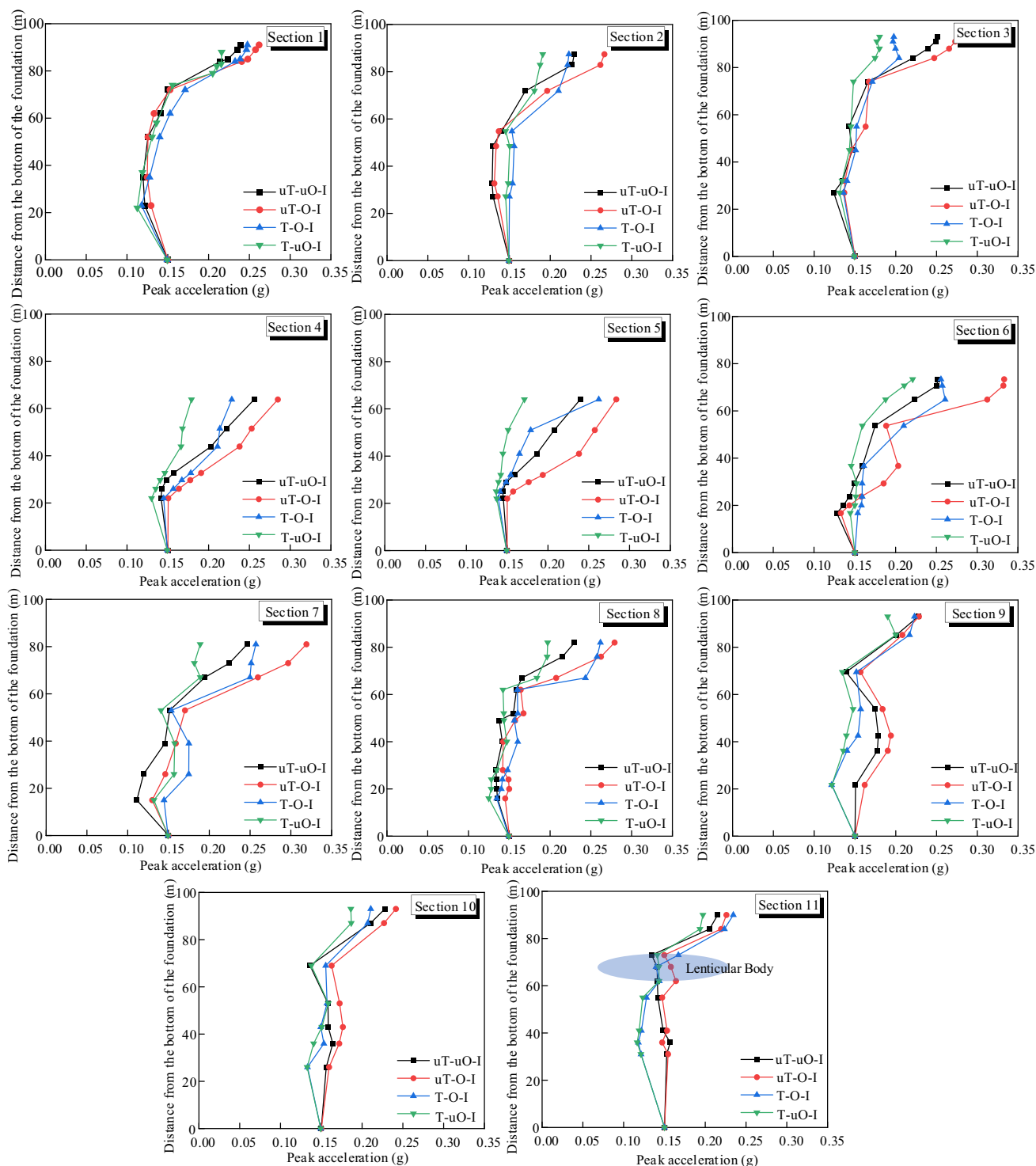**Fig. 15** Schematic of selected sections

Fig. 16 Peak acceleration along depth direction of soil layer

periods calculated by the two models at observation point 16 are equal; however, the corresponding peaks of spectral acceleration differ. The characteristic period of the slope bottom in the refined model can be initially estimated as not exceeding that in the simplified model. However, the corresponding peak spectral acceleration exceeds that of the simplified model, and the pattern of the response spectrum at the top of the slope is opposite that at the bottom of the slope. The difference between the two models mainly reflects the non-uniformity of the site.

Fig. 17 Differences in spectrum responses under different working conditions
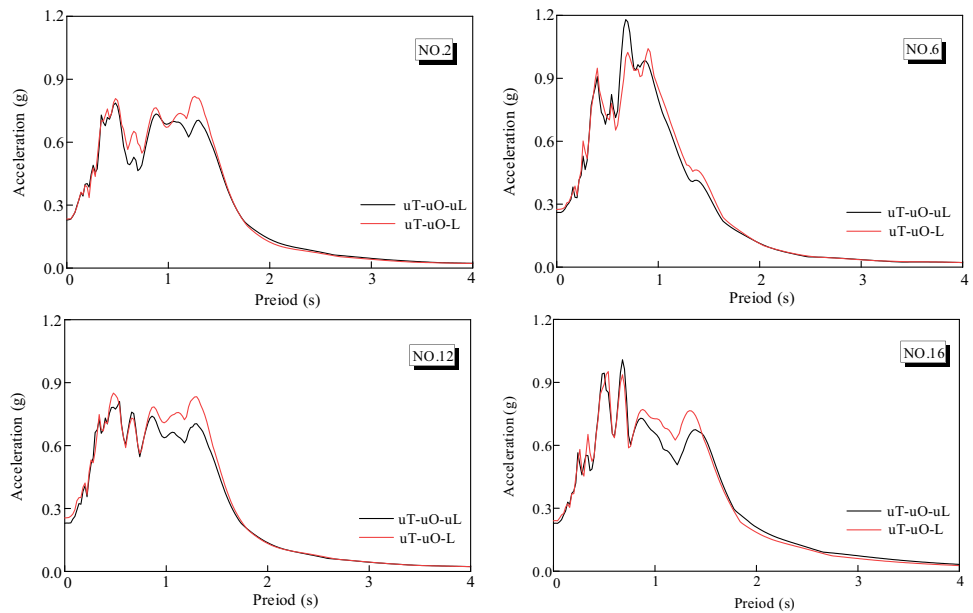

Difference in peak acceleration along depth direction

The peak acceleration curves at different depths in Sections 2, 4, 8, and 11 are plotted to investigate the variability of peak accelerations using different models along the depth direction of the soil layer, as shown in Fig. 18.

As shown in Fig. 18, the peak acceleration at different depths of the soil layer in the refined model is smaller than that in the simplified model. The change pattern of the peak acceleration curve along the depth direction of the soil layer

is fundamentally the same using different models, except for depths of 30–50 m in Section 2, 19–28 m in Section 8, and 35–40 and 70 m in Section 11. The selected sections are all located at the bottom of the slope. The topographic effect causes a certain ground motion attenuation at those locations (Gao et al. 2022), causing the peak acceleration of the refined model to be less than that of the simplified model. By considering the foregoing with the spatial distribution of soil layers shown in Fig. 15, the inclination of the interface among different soil layers at depths of 30–50 m at Section 2, 19–28 m at Section 8, and 70 m at Section 11

Fig. 18 Differences in peak accelerations along soil depth direction
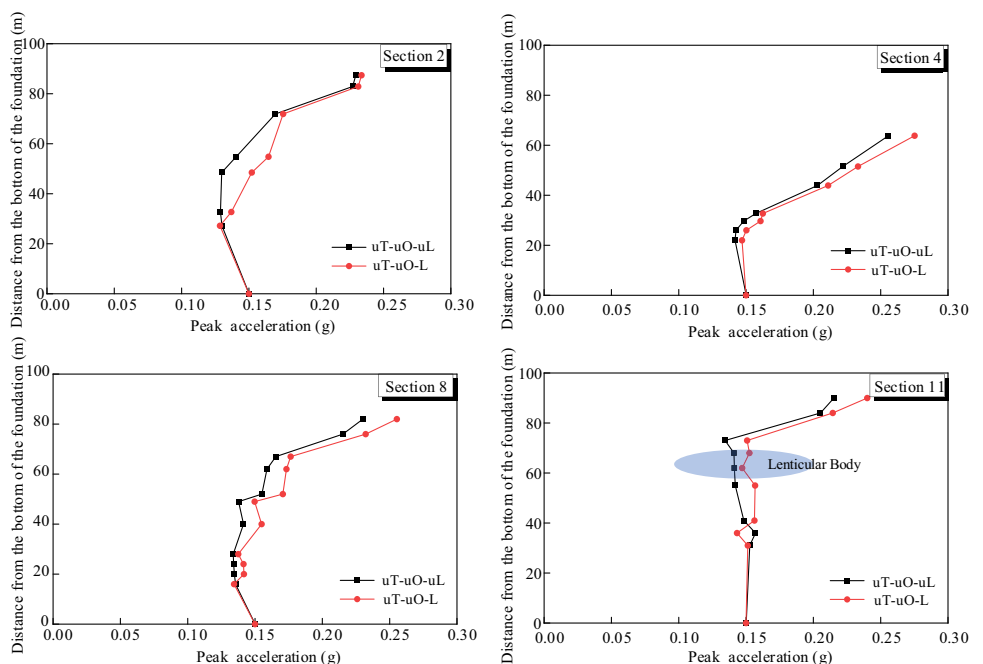
is large, and lenticular bodies exist at the 35–40 m depth in Section 11. The peak acceleration of the simplified model at the ground surface was found to be 1.9–11.5% higher than that of the refined model.

Main conclusions and discussion

A multistage slopes finite element analysis model in wide river valleys was designed. Using such model, the nonlinear seismic response of a non-uniform wide river valley site was investigated, and the spatial variability of the site seismic response was systematically analyzed. The simplified model with a horizontal soil stratum is compared with calculated results. The main conclusions and findings are as follows.

The seismic response significantly varies at different locations on the ground surface of a multistage slope and non-uniform wide river valley site. The PGA and PGV variation patterns along the ground surface were consistent with topographic relief. However, abrupt changes occur in the indices of the top of the multistage slope and location of relatively large topographic relief. The seismic response is most intense at the shoulder of the slope on both sides of the river valley. The variation in the peak acceleration along the depth direction of the soil layer is more significant when lenticular bodies exist in the stratum. The spatial variability of the seismic response at such sites is mainly related to topography and soil non-uniformity. The foregoing causes the seismic response to exhibit variability characteristics, such as amplification, attenuation, and spatial variation. Therefore, consistent ground motion input cannot be simply adopted in the seismic design of passageway engineering structures crossing multistage slopes of wide river valley sites; topographic and non-uniform site effects must be considered.

The seismic response is most intense in the non-uniform wide river valley site under the working condition that considers the overlying water pressure but ignores the traveling wave effect. The main reasons for the foregoing are related to the mutual coupling of ground motion, topographic effects, and hydrodynamic pressure. The river water is loaded on the riverbed surface in the form of pressure, and its effect on the dynamic properties of the riverbed soil is investigated. The dynamic coupling effect of river water-riverbed and the oscillation effect of water under the action of ground motion are ignored in this study. However, these affect the seismic response characteristics of the site during an actual earthquake. Therefore, the conduct of a study on the seismic response of non-uniform wide river valley sites considering the effects of the dynamic coupling of river water and riverbed as well as river water oscillation is necessary.

The response spectrum of the wide river valley site exhibits the phenomenon of "multi-peaks" and strong response over a "wide period" range. The spectral acceleration corresponding to the characteristic period of the site at the bottom of the valley exceeds that on the ground surface on both sides. The characteristic periods of the non-uniform wide river valley sites are all approximately 1.0 s, and the variability of the acceleration response spectrum on different ground surfaces of the sites is greater when the period approaches 1.0 s. According to the engineering background of large bridges built in the middle and lower reaches of the Yangtze River, the characteristic periods of these structures are also approximately 1.0 s. This indicates that the variability of the seismic response of such sites poses a serious threat to the seismic safety of bridge structures.

Significant differences were detected in the seismic response of the refined model of the wide river valley site, which considered the non-uniformity of both the topography and soil layers, in comparison to the model with a simplified horizontal soil layer. The differences were mainly concentrated at the location with large ground surface relief, at the interface among different strata with large inclinations, and near the lenticular body. Furthermore, the seismic response of the simplified model was found to be more intense than that of the refined model.

Data availability All data included in this study are available upon request by contact with the corresponding author.

Declarations

Competing interests The authors declare no competing interests.

Disclaimer All statements, results, and conclusions are those of the researchers and do not necessarily reflect the views of these foundations.

References

Anquez P, Glinsky N, Cupillard P, Caumon G (2022) Impacts of geometric model simplifications on wave propagation-application to ground motion simulation in the lower Var valley basin (France). Geophys J Int 229(01):110–137

Ashford SA, Sitar N (1997) Topographic amplification in the 1994 Northridge earthquake analysis and observations. Earthq Eng 34(1):210–214

Bao YJ, Huang Y, Zhu CQ (2021) Effects of near-fault ground motions on dynamic response of slopes based on shaking table model tests. Soil Dyn Earthq Eng 149:106869

Baron J, Primofiore I, Klin P, Vessia G, Laurenano G (2022) Investigation of topographic site effects using 3D waveform modelling: amplification, polarization and torsional motions in the case study of Arquata del Tronto (Italy). Bull Earthq Eng 20(2):677–710

Chen BK, Wang DS, Chen SL, Hu SC (2021) Influence of site factors on offshore ground motions: observed results and numerical simulation. Soil Dyn Earthq Eng 145:106729

Costanzo A, Caserta A (2019) Seismic response across the Tronto Valley (at Acquasanta Terme, AP, Marche) based on the geophysical monitoring of the 2016 Central Italy seismic sequence. Bull Eng Geol Env 78(08):5599–5616

Elgamal A, Lu JC, Forcellini D (2009) Mitigation of liquefaction-induced lateral deformation in a sloping stratum: three-dimensional numerical simulation. J Geotech Geoenviron Eng 135(11):1672–1682

Elgamal A, Lu JC, Yang ZH (2005) Liquefaction-induced settlement of shallow foundations and remediation: 3D numerical simulation. J Earthquake Eng 9:17–45

Evangelista L, del Gaudio S, Smerzini C, d'Onofrio A, Festa G, Iervolino I, Landolfi L, Paolucci R, Santo A, Silvestri F (2017) Physics-based seismic input for engineering applications: a case study in the Aterno river valley, Central Italy. Bull Earthq Eng 15(07):2645–2671

Fukushima Y, Irikura K, Uetake T, Matsumoto H (2000) Characteristics of observed peak amplitude for strong ground motion from the 1995 Hyogoken Nanbu (Kobe) earthquake. Bull Seismol Soc Am 90(03):545–565

Gao YF, Zhang N, Li DY, Liu HL, Cai YQ, Wu YX (2012) Effects of topographic amplification induced by a U-shaped canyon on seismic waves. Bull Seismol Soc Am 102(4):1748–1763

Gao GY, Li YJ, Dong WK (2018) Effect of vertical acceleration on site liquefaction in pulse ground motion. J Eng Geol 26(5):1272–1278 (in Chinese)

Gao YF, Dai DH, Zhang N (2022) Analytical study on the topographic effect on ground motion of Feitsui canyon. Acta Seismologica Sinica 44(01):40–49 (in Chinese)

Gaudiosi I, Simionato M, Mancini M, Cavinato GP, Coltella M, Razzano R, Sirianni P, Vignaroli G, Moscatelli M (2021) Evaluation of site effects at Amatrice (central Italy) after the August 24th, 2016, Mw 6.0 earthquake. Soil Dyn Earthq Eng 144:106699

Han JY, El Naggar MH, Hou BW, Du XL, Shuai Y, Li LY (2020) Nonlinear soil response under non-uniform seismic excitation from multi-point shaking table tests. Soil Dyn Earthq Eng 139:106342

Hayashi K, Burns DR, Toksöz MN (2001) Discontinuous-grid finite-difference seismic modeling including surface topography. Bull Seismol Soc Am 91(6):1750–1764

Hough SE, Altidor JR, Anglade D (2010) Localized damage caused by topographic amplification during the 2010 M 70 Haiti earthquake. Nat Geosci 3(11):778–782

Huang HC, Chiu HC (1995) The effect of canyon topography on strong ground motion at Feitsui damsite: quantitative results. Earthq Eng Struct Dyn 24(7):977–990

Huang Y, Zhu CQ (2017) Safety assessment of antiliquefaction performance of a constructed reservoir embankment. I: experimental assessment. J Perform Constr Facil 31(2):04016101

Jahromi SG, Karkhaneh S (2019) The plurality effect of topographical irregularities on site seismic response. Earthq Eng Eng Vib 18(3):521–534

Kuhlemeyer RL, Lysmer J (1973) Finite element method accuracy for wave propagation problems. Soil Mech Found Div 99:421–427

Lashgari A, Jafarian Y (2022) Empirical model for frequency content estimation of strong ground motion records of Iran. Eng Geol 297:106526

Li J, Kim K, Elgamal A (2020) Three-dimensional seismic response of a large embedded structure and induced earth pressure. J Geotech Geoenviron Eng 146(5):04020025

Li JZ, Yan JK, Peng TB, Han L (2015) Shake table studies of seismic structural systems of a Taizhou Changjiang Highway Bridge Model. J Bridg Eng 20(03):04014065

Li S, Zhang F, Wang MD, Cheng Z, Zhang Y, Zhang N, Wang JQ, Gao YF (2022) Seismic response sensitivity of a V-shaped canyon-crossing bridge considering the near-source canyon topographic effects. Soil Dyn Earthq Eng 155:107205

Liu ZX, Huang ZE, Meng SB (2022) Three-dimensional IBEM solution to seismic wave scattering by a near-fault sedimentary basin. Eng Anal Boundary Elem 140:220–242

Liu ZX, Wang D, Liang JW, Wu FJ, Wu CQ (2018) The fast multipole indirect BEM for solving high- frequency seismic wave scattering by three-dimensional superficial irregularities. Eng Anal Boun Elem 90:86–99

Lopez-Castaneda AS, Reinoso E (2021) Strong-motion duration predictive models from subduction interface earthquakes recorded in the hill zone of the Valley of Mexico. Soil Dyn Earthq Eng 114:106676

Malcioglu FS, Donmez K, Aktas YD (2022) Characteristics of strong ground motions in the 30 October 2020, M W 6.9 Aegean Sea Earthquake. Front Built Environ 8:870279

Nguyen VQ, Nizamani ZA, Park D, Kwon OS (2020) Numerical simulation of damage evolution of Daikai station during the 1995 Kobe earthquake. Eng Struct 206:110180

Ning L, Dai TY, Wang LM, Yuan SC, Pan JY (2018) Numerical investigation of Rayleigh-wave propagation on canyon topography using finite-difference method. J Appl Geophys 159:350–361

Primofiore I, Baron J, Klin P, Laurenzano G, Muraro C, Capotorti F, Amanti M, Vessia G (2020) 3D numerical modelling for interpreting topographic effects in rocky hills for seismic microzonation: the case study of Arquata del Tronto hamlet. Eng Geol 279:105868

Rietbrock A (2001) P wave attenuation structure in the fault area of the 1995 Kobe earthquake. J Geophys Res-Solid Earth 106(B3):4141–4154

Sahoo PP, Shukla SK (2021) Time-history analysis of soil slope subjected to seismic loadings. Soil Mech Found Eng 58(2):130–137

Sohrabi-Bidar A, Kamalian M, Jafari MK (2010) Seismic response of 3D Gaussian-shaped valleys to vertically propagating incident waves. Geophys J Int 183(3):1429–1442

Taboada-Urtuzuastegui VM, Martinez-Ramirez G, Abdoun T (2002) Centrifuge modeling of seismic behavior of a slope in liquefiable soil. Soil Dyn Earthq Eng 22(9):1043–1049

Trifunac MD, Hudson DE (1971) Analysis of the Pacoima dam accelerogram-San Fernando, California, earthquake of 1971. Bull Seismol Soc Am 61(5):1393–1141

Wang LM, Xu YX, Xia JH, Luo YH (2015) Effect of near-surface topography on high-frequency Rayleigh-wave propagation. J Appl Geophys 116:93–103

Wang H, Luo C, Wan JZ, Zhu MF, Lou ML, Feng HP (2021a) A hybrid boundary method for seismic wave propagation problems in slopes. Soil Dyn Earthq Eng 147:106773

Wang HL, Yan SM, Liu ZX, Cheng XL (2021b) Amplification effect of ground motion in offshore meandering sedimentary valley. Shock Vib 2021:6932976

Wang W, Li DQ, Liu Y, Du WQ (2021c) Influence of ground motion duration on the seismic performance of earth slopes based on numerical analysis. Soil Dyn Earthq Eng 143:106595

Wei X, Yang J (2019) Characterizing the effects of fines on the liquefaction resistance of silty sands. Soils Found 59(06):1800–1812

Wang ZH, Saito Y, Hori K, Kitamura A, Chen ZY (2005) Yangtze offshore, China: highly laminated sediments from the transition zone between subaqueous delta and the continental shelf. Estuar Coast Shelf Sci 62(1–2):161–168

Xie JJ, Zimmaro P, Li XJ, Wen ZP (2017) Rupture directivity effects on strong ground motion during the 15 April 2016 M-w 7.0 Kumamoto Earthquake in Japan. Bull Seismol Soc Am 107(03):1265–1276

Yang CW, Zhang L, Liu Y, Tian DH, Guo XY, Liu Y (2020) Shaking table test on dynamic response of bedding rock slopes with weak structural plane under earthquake. Front Phys 8:556714

Yang J, Zhuang HY, Wang W, Zhou ZH, Chen GX (2021) Seismic performance and effective isolation of a large multilayered underground subway station. Soil Dyn Earthq Eng 142:106560

Zhang N, Zhang Y, Dai DH (2021) Dynamic response of a functionally graded cylindrical tube with power-law varying properties due to SH-waves. Waves Random Complex Media 2021:1948628

Zhang N, Zhang Y, Gao YF, Pak RYS, Wu YX, Zhang F (2019) An exact solution for SH-wave scattering by a radially multilayered inhomogeneous semicylindrical canyon. Geophys J Int 217(2):1232–1260

Zhu CQ, Cheng HL, Bao YJ, Chen ZY, Huang Y (2022) Shaking table tests on the seismic response of slopes to near-fault ground motion. Geomech Eng 29(2):133–143

Zhu CQ, Huang Y (2017) Safety assessment of antiliquefaction performance of a constructed reservoir embankment. II: numerical assessment. J Perform Constr Facil 31(2):04016102

Zhuang HY, Chen GX (2006) A viscous-plastic model for soft soil under cyclic loadings. In: Geotechnical Special Publication of ASCE, Soil and Rock Behavior and Modeling -Proceedings of the Geo-Shanghai Conference 150:343-50

Zhuang HY, Wang R, Chen GX, Miao Y, Zhao K (2018) Shear modulus reduction of saturated sand under large liquefaction-induced deformation in cyclic torsional shear tests. Eng Geol 240:110–122

Zhuang HY, Wang R, Shi PX, Chen GX (2019) Seismic response and damage analysis of underground structures considering the effect of concrete diaphragm wall. Soil Dyn Earthq Eng 116:278–288

Zhuang HY, Wu XZ, Chen GX (2011) Study of nonlinear static and dynamic coupling interaction of soil-underground structure considering initial static stress. Chin J Rock Mech Eng 30(Suppl. 1):3112–3119 (in Chinese)

Zhuang HY, Yang J, Chen S, Dong ZF, Chen GX (2021) Statistical numerical method for determining seismic performance and fragility of shallow-buried underground structure. Tunn Undergr Space Technol 116:104090

Zhuang HY, Yang J, Chen S, Li HX, Zhao K, Chen GX (2020) Liquefaction performance and deformation of slightly sloping site in floodplains of the lower reaches of Yangtze River. Ocean Eng 217(11):107869